Time-dependent traction force microscopy for cancer cells as a measure of invasiveness

Valentina Peschetola, Valérie M. Laurent, Alain Duperray, Richard Michel, Davide Ambrosi, Luigi Preziosi, Claude Verdier

Time–dependent traction force microscopy for cancer cells as a measure of invasiveness

Valentina Peschetola[1,5], Valérie Laurent[1], Alain Duperray[2,3], Richard Michel[1]
Davide Ambrosi[4], Luigi Preziosi[5], Claude Verdier[1*]

(1) CNRS / Univ. Grenoble 1, LIPhy UMR 5588, Grenoble, F-38041, France
(2) INSERM U823, Grenoble, France
(3) Univ. Grenoble 1, Faculté de Médecine, Institut d'oncologie/développement, Albert Bonniot et Institut Français du Sang, UMR-S823, Grenoble, France
(4) MOX - Dipartimento di Matematica, Politecnico di Milano, Piazza Leonardo da Vinci 32, 20131 Milano, Italy
(5) Department of Mathematics Politecnico di Torino, Corso Duca degli Abruzzi 24, 10129 Torino, Italy

Abstract

The migration of tumor cells of different invasivity is studied, and traction forces are determined in time on soft substrates (Young modulus 10 kPa). It is found that the outliers of the traction stresses are quite relevant to differentiate different cancer cell lines which are more or less invasive. Here we tested two different epithelial bladder cancer cell lines, one invasive (T24), and a less invasive one (RT112). Invasive cancer cells move in a nearly periodic motion, with peaks in velocity corresponding to higher traction forces exerted on the substrate, whereas the less invasive cell develops almost constant time–dependent traction stresses. The dynamics of focal adhesions as well as cytoskeleton features reveal different mechanisms activated to migrate, depending on their invasiveness. T24 invasive cells show an interconnected cytoskeleton linked to mature adhesion sites, leading to small traction stresses, whereas less invasive cells (RT112) show a less–structured cytoskeleton, unmature adhesions corresponding to higher traction stresses. Migration velocities are smaller in the case of less invasive cells. The MSD (Mean Squared Displacement) shows super–diffusive motions with a higher exponent for the more invasive cancer cells. Further correlations between traction forces and the actin cytoskeleton reveal an unexpected pattern with a large actin rim at the RT112 cell edge where higher forces are colocalized, whereas a more usual cytoskeleton with stress fibers and focal adhesions is found for T24 cancer cells. Thus the method can be an interesting one to differentiate cancer cell invasiveness.

Keywords : cancer cells, traction forces, invasiveness, adhesion, migration, MSD.

*Corresponding author, claude.verdier@ujf-grenoble.fr

1 Introduction

Cell migration has been studied for many years and it is known that the shape of cells during motion obeys to multiscale processes (time and space) [31]. Most of them involve cytoskeleton changes driven by the actin machinery [46] in relation with the values of traction forces exerted on the substrate [4, 13, 17]. These seem to correlate with the development of focal complexes [4, 19, 23]. The cell velocity of migration is connected with its ability to form/break bonds on substrates and contract its own body to move forward. But it has also been shown [24] that rapid migration does not always correspond to an organized system between actin, myosin II and focal adhesions (FAs).

Although it is now possible to determine traction forces in three dimensions [37, 34, 12] with the arrival of new microscopy techniques [18, 29], most studies have focused on plane polymeric substrates. PA (PolyAcrylamide) substrates coated properly with Extra–Cellular Matrix (ECM) components such as fibronectin or collagen are an efficient tool. Recent techniques involve the production of micropatterns (soft lithography) of controlled shape [56] to increase the number of analyzed cells. On the other hand, such methods force cells to adhere at specific places with a controlled shape.

Traction forces methods couple inverse problems and microscopy in order to access the local values of forces/displacements developped by cells. Most methods use embedded fluorescent beads in PA substrates, then correlation techniques are used to reconstruct the displacement field. All methods need a regularization (usually the Tikhonov scheme) and adequate filtering of the data. Four main methods are currently available to do so: Traction Reconstruction with Point Forces (TRPF) [50], Fourier Transform Traction Cytometry (FTTC) [8], the classical Boundary Element Method (BEM) [13] and the more recent Adjoint Method (AM) [1, 2]. A recent work by Sabass and coauthors [48] gives a comparison between the first three methods and shows how to improve them by adequate filtering and regularization. Similarly, improvements in the resolution are also available by comparing FTTC and TRPF methods [54]. Other methods have been proposed earlier for measuring forces, such as the use of wrinkled patterns on soft PDMS [26, 7] or the deformation of microposts [55]. Wrinkled patterns do not provide traction maps or are difficult to analyze, and microposts use a direct method but provide a non–continuous environment, so we will rather focus here on the previous 2D methods on soft substrates, using the AM method.

Several authors studied the effect of substrate rigidity [36, 15, 21, 2], substrate anisotropy [49] and topography [22], as well as the effect of ECM protein density [42]. Cells are known to migrate more efficiently on rigid substrates [36], although this phenomenon is cell–dependent [15], and

the velocity of migration seems to find an optimum for a specific matrix protein concentration [42]. This behavior is related to strength stiffening of the integrin–cytoskeleton bonds [9] with matrix rigidity. Focal adhesions are indeed connected through the integrin bounds, their size being proportional to the applied forces [4]. Nevertheless, it seems that this linear relation is only valid at short times [53] when myosin–mediated contractions and focal maturation are at work, and that long term adhesion (with mature adhesions) does not exhibit this correlation.

Although these methods are quite promising and provide adequate tools for linking forces with cytoskeleton and focal complexes, more research is still needed to understand the precise mechanisms by which cells migrate in time. In particular, few studies involve cancer cells on 2D–substrates or lead to contradictory results [39, 28, 32], and it could be interesting to find *in vitro* methods for characterizing cell migration speed, applied forces, and subsequent fluorescence images of their cytoskeleton and focal complexes in time. It is indeed possible that cancer cells develop particular forces and develop precise adhesion mechanisms to propel themselves through tissues or when extravasating. Such observations were initially proposed by Munevar *et al.* [41] when they compared fibroblasts with (H-ras) transformed cells: the latter ones showed smaller traction forces, and a disorganized motile behavior. Recently Indra and coworkers [28] also found inverse correlation between traction forces/adhesion strength and the metastatic potential of different cancer cells, but Kraning-Rush *et al.* [32] on the other hand found opposite results.

Here we provide more detailed time–dependent behavior of two cancer cell lines (T24 and RT112, which are epithelial bladder cell lines) and measure the traction forces exerted on PA substrates coated with collagen. These features are compared with complementary migration assays to determine migration velocities, then fluorescence microscopy enables us to quantify the cytoskeleton changes as well as focal adhesions. Finally traction force locations are investigated together with the actin changes, to determine the precise migration patterns of these two cells. Section 2 presents the materials and methods used in this work. In section 3, the main results are illustrated concerning traction forces, immunofluorescence and migration velocities. Finally, results are compared and discussed in section 4.

2 Materials and methods

2.1 Cell culture

Epithelial bladder cancer cell lines have been used in this study. These cells were obtained from ATTC (Rockville, USA) and were cultured in RPMI 1640 (Sigma Chemical Co.) supplemented with 10% fetal bovine serum and antibiotics. Cultures were kept at 37°C in 5% CO_2 humidified

atmosphere. In particular, two bladder carcinoma cell lines have been investigated: T24 and RT112. T24 cancer cells are poorly differentiated and have a cytological grade 3. The RT112 line is a moderately differentiated one and is characterized by cytological grade 2. *In vitro*, T24 cells display a high invasive capacity, whereas RT112 cells present a moderate invasive capacity [5, 30].

Cells are seeded on the Polyacrylamide gel (see below) and left overnight to spread. Then images are made every other minute over long periods of time, up to 2 hours.

2.2 Gel preparation

A protocol similar to the one suggested earlier [13, 44] has been used to make 10 kPa PA gels. A square coverglass (22 mm × 22 mm) is treated with silane (Sigmacote SL-2) for 30 minutes. Round coverglasses (35 mm diameter) are washed with 0.1M NaOH, treated with APTMS for 10 minutes, washed with PBS twice and treated with 200 µl of 0.5% glutaraldehyde for 30 minutes. A 0.5 ml gel solution is prepared, containing 30% acrylamide (166 µl), 1% bis–acrylamide (14 µl) in distilled water (314 µl). Fluorescent beads (Molecular Probes, 0.2 µm in diameter) are seeded into the solution before addition of the crosslinkers (2.5 µl of APS and 0.5 µl of TEMED). Overall, the gel contains 10% acrylamide and 0.03% bis–acrylamide. The adequate amount of solution (corresponding to a 70 µm gel thickness) is put onto the square coverglass. The circular coverglass is brought carefully from the top to capture the gel solution by capillarity, thus avoiding to flip the preparation. The gel is left to polymerize for nearly 90 minutes. After polymerization, the square coverglass is gently removed. In this protocol, Sulfo–Sanpah is used to covalently bind the protein (collagen) to the polyacrylamide surface. The gel is covered with 200 µl of a Sulfo–Sanpah solution (Sulfo–Sanpah 1mM, DMSO and HEPES at pH=8.5), then exposed to a UV lamp (2×15 Watts) for 2 mn: this enables to activate Sulfo–Sanpah molecules, so that they bind collagen. This process is repeated twice, then 200 µl of the collagen solution (100 µg/ml) are applied and let overnight to bind the activated Sulfo-Sanpah at 4 °C.

The mechanical gel properties have been determined previously [2] and the specific gel used throughout this study (10% acrylamide-0.03% bis–acrylamide) has an elastic Young modulus $E = 10$ kPa as determined by rheometry, assuming that $\nu = 0.5$ (Poisson coefficient). This was also checked using AFM measurements [45]. The gel roughness was shown to be around 100 nm as shown using AFM contact mode. Note that this gel rigidity was selected as a compromise between a similar environment for cells as the one they are subjected to, but also aiming at minimizing possible three–dimensional deformations that could occur for too soft gels. The value of 10 kPa appeared to met these two conditions, and displacements were also easily detected (usually a few µm).

2.3 Traction forces

The mechanical characterization of the gel is approximated as isotropic and elastic and the displacements are observed to be small enough so that linear elasticity applies. The gel depth (usually 70 µm) is large enough so that it can be approximated by a half space. Since the response of the substrate is linear, the displacement $\mathbf{u}(\mathbf{r})$ at position $\mathbf{r}$ can be related to the traction field $\mathbf{t}(\mathbf{r})$ at the boundary ($x_3 = 0$) of the 3D–gel via the integral:

$$\mathbf{u}(\mathbf{r}) = \int \mathbf{G}(\mathbf{r} - \mathbf{r}')\,\mathbf{t}(\mathbf{r}')\,\mathrm{d}s(\mathbf{r}') \tag{1}$$

where $\mathbf{G}$ is the Green's tensor for the Boussinesq–Cerruti problem [33]. In the particular case where (1) is used for $\mathbf{r} = (x_1, x_2, 0)$ and pure shear $\mathbf{t} = (t_1, t_2, 0)$, $\mathbf{G}(\mathbf{r})$ takes the form:

$$\mathbf{G}(\mathbf{r}) = \frac{1+\nu}{\pi E}\left((1-\nu)\,\frac{\mathbf{1}}{r} + \nu\,\frac{\mathbf{r}\otimes\mathbf{r}}{r^3}\right) \tag{2}$$

where r is the magnitude of $\mathbf{r}$, E is the elastic modulus and ν is the Poisson ratio.

In this work we use the adjoint method, whose details are given in previous works [1, 2]. We recall that first, the problem is reduced to a 2D–one by averaging along an effective thickness h (in the x_3 direction). Secondly, the tractions are determined by a minimization technique, in the spirit of Lions [35]. The solution consists in solving the following partial differential equations and boundary conditions with unknowns $\mathbf{u}$ and the intermediate variable $\mathbf{p}$:

$$-\mu\Delta\mathbf{u} - (\mu+\lambda)\,\nabla(\nabla.\mathbf{u}) = -\frac{\chi_\mathrm{c}}{\varepsilon}(\mathbf{p} - \bar{\mathbf{p}}) \quad \text{in} \quad \Omega_\mathrm{c}, \qquad \mathbf{u} = \mathbf{0} \quad \text{on} \quad \partial\Omega_\mathrm{c} \tag{3}$$

$$-\mu\Delta\mathbf{p} - (\mu+\lambda)\,\nabla(\nabla.\mathbf{p}) = \chi_0(\mathbf{u} - \mathbf{u_0}) \quad \text{in} \quad \Omega_\mathrm{c}, \qquad \mathbf{p} = \mathbf{0} \quad \text{on} \quad \partial\Omega_\mathrm{c} \tag{4}$$

Finally the traction field $\mathbf{t}$ is given by $\mathbf{t} = -\frac{\chi_\mathrm{c}}{\varepsilon}(\mathbf{p} - \bar{\mathbf{p}})$ [45], which ensures that the traction forces are null outside the cell, and that the resulting force on the cell is zero: $\int_{\Omega_\mathrm{c}} \mathbf{t}\mathrm{d}s = \mathbf{0}$.

In the above equations, $\bar{\mathbf{p}} = \frac{1}{|\Omega_\mathrm{c}|}\int_{\Omega_\mathrm{c}} \mathbf{p}\mathrm{d}s$, χ_c and χ_0 are characteristic functions associated to Ω_c (cell region) and Ω_0 (where beads displacements are known), $\mathbf{u_0}$ is the known displacement, $\mu = \frac{hE}{2(1+\nu)}$ and $\lambda = \frac{hE\nu}{1-\nu^2}$ are the reduced 2D–Lamé coefficients (plane stress model). h is chosen as the height within which beads move (typically $h = 1.5\,\mu\mathrm{m}$). ε is the regularization parameter to be optimized using the L–curve technique [1, 45]. We used $\varepsilon = 6 \times 10^{-7}$ in our case.

The observed displacement $\mathbf{u_0}$ is obtained from fluorescent images of the beads near the gel surface. The initial bead positions are recovered at the end of the experiment by adding distilled water in the culture medium, which makes cells to detach and the gel eventually relaxes. Then

the displacement $\mathbf{u_0}$ can be calculated, thanks to the graph technique routine 'Particle–Tracker' available from the ImageJ software [47].

The system of equations (3-4) is solved using a finite element method with elements nodes matching the beads positions. Then linear basis functions are used on an unstructured mesh. A global biconjugate gradient method has been used to solve the resulting linear system numerically.

For calculating the resultant of the stresses within the lamellipodium, the direction of migration is determined by following the trajectory of the center of mass, then the resultant force is computed by summation of the stresses times the surface element area (from the finite element mesh) to obtain a force in Newtons. Time–dependent results have been obtained by following cell trajectories, and the mean value is taken from this data.

2.4 Cell migration on gels and Mean Squared Displacement (MSD)

Gels were made similarly as described above for the long–term migration experiments. Special Petri dishes with a coverglass glued at the bottom were specially made and PA gels (10 kPa) were prepared inside. Cells were seeded on the gels and the same culture medium was added in the Petri dish. Visualization of several cells properly chosen were made in time, and followed over 2 hours generally. The geometric center was calculated and its position in time was recorded. Then the Mean Squared Displacement (MSD) was calculated according to the formula below:

$$\mathrm{MSD}(t) = < |\mathbf{r}(t+\tau) - \mathbf{r}(\tau)|^2 >_\tau \tag{5}$$

where the averaging brackets <> are taken for all possible time lags τ ($0 \leq \tau \leq t$).

The behavior of this MSD in time was analyzed by looking at the power dependence of $\mathrm{MSD(t)} \sim t^\alpha$, where α is the time–exponent or persistence parameter. It is known that values of $\alpha < 1$ correspond to subdiffusive motions, $\alpha = 1$ means diffusive motion, whereas $\alpha > 1$ is a superdiffusive motion. The case $\alpha = 2$ is called the ballistic case (directional motion). Such exponents were measured during the migration assay and the final value of α was chosen as the time–average value.

The behavior of the MSD is an important feature of the cell migration process, as shown recently [14] because it can allow to determine the signature of a particular cell to migrate, change direction or polarize over long periods of time.

2.5 Immunofluorescence and confocal microscopy

Briefly, after being washed with PBS, cells were fixed using PFA (paraformaldehyde 3% in PBS) for 10 min, permeabilized with PBS containing 0.5% Triton X100 for 10 min, and then washed with PBS containing 0.2% saponin and 2% BSA. Fixed cells were then incubated with rabbit anti–myosin IIA (Biomedical Technologies Inc., USA) and mouse anti–human paxillin (clone 5H11, from Upstate Biotechnology, USA) for 30 min, and washed with PBS containing 0.2% saponin and 2% BSA. Cells were then stained with phalloidin Alexa Fluor-488 for actin, Hoechst 33342 for nuclei, Donkey anti-rabbit IgG (conjugated with Dylight 649, Jackson ImmunoResearch, USA), and Goat anti-Mouse IgG (labelled with Alexa Fluor–546, Molecular Probes, The Netherlands). The samples were imaged using a Zeiss 710 confocal microscope.

Live cell imaging was carried out on a confocal microscope (Zeiss LSM) at the Institut Albert Bonniot. T24 and RT112 cells were transfected for actin–GFP and time acquisitions were made every two minutes, simultaneously with the fluorescent beads (red) acquisition. Thus correlations between actin localization and traction forces could be made. Co–localization analysis was made using the ImageJ software [47].

3 Results

Time dependence of traction forces

An image showing a T24 cell on a PA substrate is shown in Fig. 1. Note that this cell develops a large lamellipodium and migrates from the left to right (see also supplemental movie $S1$). A traction force map at this characteristic time (t = 6 mn corresponding to the active migration pattern in Fig. 2) is also shown. Forces (per unit surface) developped by this type of cancer cell reach maximum values in the range of 150 Pa.

This phenomenon was shown to be time–dependent [2, 53], as cells usually pull on their focal adhesions to propell themselves, then they relax. This dynamics is shown in Fig. 2 where a time–dependent process is depicted over 40 minutes. All values of stress magnitude are reported in the form of a boxplot for each time. This information is also presented in the supplemental movie $S2$. As seen previously for this type of cell [2], T24 cells usually exhibit a periodic motion, pulling strongly then relaxing stresses, over and over. This type of motion is a so called five–step process (mesenchymal motion), involving the development of protrusions, formation of adhesions and pulling, cell contraction, release of bonds at the rear and recycling [52]. Note that a large number of outliers[1] are present and correspond to the higher forces developped at focal sites. This

[1] values located outside the interval $[Q_1 - \alpha\,(Q_3 - Q_1); Q_3 + \alpha\,(Q_3 - Q_1)]$, where Q_1 is the lower quartile, Q_3

will be studied below.

A similar set of results in the case of less invasive RT112 cancer cells, is shown in Fig. 3. The cell has a round shape, more likely to resemble an ameboid type of motion (see also supplemental movie $S3$). Tractions are more homogeneous, and the values appear to be larger than for T24 cells. This higher value is also repeated in time as can be observed in Fig. 4. But the observed values of the outliers over 78 minutes do not appear to change much. This information is also presented in the supplemental movie $S4$.

To compare the motion of the two types of cancer cells, only higher values i.e. outliers (corresponding to probable focal complexes [4]) are retained in Fig. 5. RT112 cells develop higher average values of outliers (around 170 Pa) as compared to T24 cells (120 Pa). This analysis was carried out for $N = 9$ cells of each type and by averaging results for all times. This result is in agreement with previous works [41, 28] and could describe a possible way for invasive cells to move rapidly without exerting too large forces.

Global force exerted on half–cell

The total force developped in the direction of migration by cancer cells on the PA substrate is calculated for a half cell only (indeed the resultant force over the cell domain is zero, i.e. $\int_{\Omega_c} \mathbf{t}\, \mathrm{d}s = \mathbf{0}$ so one has to consider the sum of stresses in a half–cell to obtain a relevant result) and is shown in Fig. 6. One can estimate the difference between T24 and RT112 cells. Forces are concentrated at the leading edge or within the lamellipodium for T24 cancer cells, whereas centripetal stresses are located all around the edges in the case of the RT112 cell, a migration behavior similar to some keratocytes [6].

Immunofluorescence: focal adhesions, actin and myosin

Immunofluorescence experiments are reported in figures 7–8. The development of the actin structure (in green, using staining with Phalloidin Alexa 488) can be seen, then the localization of the focal adhesion complexes is shown (in red, using an anti–paxillin antibody) as well as myosin motors (in magenta, using an antibody for myosin IIA), and finally the composite picture showing all sub–structures is presented. Note that nuclei were also stained in blue (using Hoechst for DNA).

The two cell types exhibit different aspects. T24 cells show a thin cytoskeleton localized close to the edges with interconnected stress fibers throughout the whole cell, whereas RT112 cells exhibit a wider actin network close to the edges.

T24 cells show larger focal complexes, as evidenced by the paxillin staining, thus allowing for a more efficient motion. This is confirmed by quantitative analysis of the total area of focal

the higher quartile, and $\alpha = 1.5$

complexes, which was made relevant by normalizing with cell area. After careful analysis of several cells (N=9 for each cell line), the contours of focal areas were determined and only large focal areas (>0.5 µm^2) were kept. It was shown that T24 cells present significant larger focal areas (1.13 µm^2) as compared to RT112 cells (0.86 µm^2), see also Table 1 below. But T24 cells have a larger spreading area (2200 µm^2, as compared to 1600 µm^2 for RT112 cells) on PA gels. The average of the ratio $FAs/A(\%)$ (ratio of total focal areas FAs over cell area A) was plotted as a bar–plot in Fig. 9, and this average is slightly higher for T24 cells. Apparently those RT112 cells develop a smaller amount of focal complexes on soft gels, and therefore cannot move efficiently: they are more likely to move slowly than undergo rapid migration. Note that similar focal areas, showing periodic spatial fingers at the edges, have been observed previously when applying mechanical stresses [43] or under flow [11].

Actin and myosin are co–localized at some locations of the periphery of T24 and RT112 cells, see Fig. 7 and Fig. 8. Actin fibers organize in a cortical structure going through the locations of focal adhesions, and similarly for Myosin IIA, especially for RT112 cells (Fig. 8). This seems to correlate with the development of large forces. In the case of T24 invasive cells, the organization of the actin cortex shows interconnections over the whole cell body, as for Myosin IIA. There are larger adhesion sites than with RT112 cells. Regarding colocalization of actin and myosin, it is clear from Figure 8 that a larger cortex of acto–myosin is shown in the case of RT112 cells (thickness around 5 µm), whereas T24 cells (Figure 7) only show thin acto–myosin structures (1–2 µm) at the cell rims. This will be discussed in the next section.

Cell migration and MSD

The migration process of the two cell types (T24 and RT112) can be described in terms of the MSD function, as well as the velocity of migration. The MSD was determined as explained above, and the velocity of migration was chosen as the total cumulative distance in order to detect cells going back and forth over long times. Actually, the instantaneous velocity may over–estimate this velocity in the case of cells moving rapidly for limited times (as for example when they pull on their lamellipodium in order to move forward). A clear difference between the two cell types appears, i.e. the persistence parameter α is found to be larger for T24 cells, equal to 1.57 whereas it is only 1.21 for the less invasive RT112 cells (N=9). The velocity of migration follows the same trend and shows more rapid invasive T24 cancer cells ($V = 0.38\,\mu$m/mn) as compared to the slow RT112 cells ($V = 0.17\,\mu$m/mn).

4 Discussion

The main results reported above are summarized in Table 1:

Cell type	Cyt. grade	σ (Pa)	F(nN)	$FAs/A(\%)$	$FAs(\mu m^2)$	V(µm/mn)	α
T24	G3	120	17.4	0.98	1.13	0.38	1.57
RT112	G2	171	22.8	0.89	0.86	0.17	1.21
p	-	(**)	0.14	0.4	(***)	(***)	(***)

Table 1: Summary of dynamic and kinematic quantities obtained for T24 and RT112 cells. p is the significance. (*) p< 0.05, (**) p< 0.01 and (***) for p< 0.001.

The values reported in the table are the cell cytological grade, the average magnitude of traction stresses outliers σ (in Pa), the average magnitude of the resultant force F (nN) developped on a half–cell, the ratio of focal adhesions to cell area $FAs/A(\%)$, the focal adhesions average area $FAs(\mu m^2)$, the migration velocity V(µm/mn), and finally α, the exponent from the MSD relationship in Eq. 5. The value of the significance parameter p is also indicated.

As was pointed out before, few studies have focused on the comparison between different cell lines behaviors on soft gels. Munevar et al. [41] considered normal and H–ras transformed 3T3 fibroblasts and showed a strange behavior of H–ras fibroblasts which did not develop stable forces but rather disorganized values around the cell edges during motion. The same behavior is observed in this work with an increase of traction stresses with the less invasive cells (Fig. 5–6).

Another important aspect investigated here is the time–dependence of the traction forces for the two cell types observed in Fig. 2 and Fig. 4. It can be mentioned that outliers represented in these figures contain the information on the large forces developped at focal sites. It is found that the dynamics of outlier forces correspond to a classical five–step process [52] in the case of T24 cancer cells, as already noticed [2]: forces peaks (as observed in Fig. 2) range from 80 Pa to 150 Pa roughly, with an average around 120 Pa (Table 1). On the other hand, RT112 cells present outliers (in the time range considered) which remain rather constant (Fig. 4), equal to 171 Pa (Table 1), with very small fluctuations. This suggests that the mode of motion described is a continuous one, where adhesions are rather rapidly formed and broken. This is also confirmed by inspection of Fig. 6, where local stresses on both sides of RT112 cells cancel out to give a resultant force in the direction of migration, as observed previously for keratocytes [6]. Therefore, a clear distinct mechanism of migration was observed for each cell type and quantified.

To confirm these assumptions, we discuss the location, number and size of focal adhesions (Fig. 9); they are known to be linked to the cytoskeleton, in particular the actin filaments. We

chose to quantify the total area of such paxillin–rich domains, in particular those with size larger than $0.5\,\mu m^2$ (mature adhesion sites). Only the percentage of focal areas with respect to cell size is shown and, interestingly, this number (around 1% for T24 cells, and 0.9% for RT112 cells, see Fig. 9) increases with cell invasivity. Moreover, larger adhesion sites ($1.13\ \mu m^2$) are found for T24 cells as compared to RT112 cells ($0.86\ \mu m^2$, see Table 1). In the work of Indra *et al.* [28], adhesion centrifugation assays conducted on harder PA gels showed a smaller number of adhering cells when metastatic capacity increased, but focal adhesions were only shown on glass substrates, therefore results are difficult to compare regarding size and numbers of focal adhesions. Nevertheless, our data on adhesion shows that traction forces are not proportional to focal adhesion areas, a framework previously described earlier [53] in the early stages of myosin–mediated maturation of adhesions. This means that this data concerns probably cells showing focal adhesions at a different level of maturation, probably more mature ones, as was postulated initially.

Next we discuss the cytoskeleton role by studying fluorescent actin–images, and their correlation with the myosin and paxillin sub–structures in Figs 7–8. This is motivated by the correlation between actin and myosin which can enable cell contractions and change their motility (see for example [3]). Another correlation is between traction forces and the actin flow [20] in regions where large focal areas exist and where the actin flow is small (and conversely). Finally the myosin activity is usually linked to focal adhesions formation in the actin–rich lamellipodium [23]. In the images showing myosin IIA and the actin network (Figs 7–8), it can be seen that the myosin IIA density is particularly enhanced at the leading edge of the cancer cells, and that it corresponds to the rich actin domains. On the other hand, the actin and myosin regions are thinner in the case of T24 cells (usually 1–2 μm wide), whereas they are much larger for RT112 cells (around $5\,\mu m$) thus allowing more acto–myosin contractions for the latter cells. This feature is in favor of the larger stresses found for RT112 cells.

Finally focal areas located at the leading edge of T24 or RT112 cells also differ: they seem to be well connected to the actin and myosin networks for T24 cells, whereas they do not appear to be so well colocalized for RT112 cells. This would mean that focal complexes are more mature ones [53] in the case of a less invasive RT112 cell which spreads rather than migrates. On the contrary, T24 cells may develop their mature adhesions rapidly and renew them faster, which makes them migrate more rapidly.

In terms of cell migration, the MSD analysis showed that T24 cells move more rapidly than less invasive RT112 cells and that their persistence exponent α is larger (1.57 for T24 cells *vs*. 1.21 for RT112 cells). It cannot be concluded that this is always true, but this gel rigidity seems to enable us to discriminate such cells. The exponent of T24 cell is similar to the ones found by Dieterich *et*

al. [14] who measured super–diffusive behaviors as well (α around 1.5).

Finally, it is important to compare traction force microscopy (TFM) with the evolution of the actin cytoskeleton [58]. This was achieved thanks to actin–GFP transfected T24 and RT112 cells, and observations of the migration behavior was followed in time as before. Figures 10-11 show images of both the actin filaments and the magnitude of the forces developped by the two cancer cells. A good correlation appears between the actin structure and the high levels of forces. In particular, Figure 11 shows a particularly large actin cortex developped by RT112 cells at the front, as seen before (Fig. 8). The larger forces are also located in that area which explains the way this type of cell moves. On the contrary, T24 cells as in Fig. 10 show a thinner cortex (same as previously, Fig. 7) with orientation parallel to cell edges. This can be shown in the comparison of the intensity levels shown along the two lines in Figures 10-11 where a more defined actin intensity is seen at the cell edges for the T24 cell, whereas the actin cortex is wider for the RT112 cell. This result brings the idea that the two types of motion correspond to a clear different motility behavior: pulling at the front on adhesion sites for T24 cells, whereas RT112 cells pull on the sides thanks to larger acto–myosin complexes and use less adhesion.

This effect is detailed in Figure 12 where colocalization of the actin intensity is compared with the magnitude of traction stresses. As can be shown in these two figures, colocalization of actin (in green) and force (in red) is strong at leading edge of T24 cell, whereas it is located in wider areas in the case of the RT112 cell (see also supplemental movies $S5$ and $S6$ for a more detailed time–dependent process). As suggested before, this feature seems to indicate that RT112 cells move by using large lateral contractions due to the presence of a wide acto–myosin cortex, whereas T24 cells only use protrusions at the leading edge where the acto–myosin cortex is more efficient. This is a possible way to explain differences in the invasiveness of such cells. Finally the ability to move faster might be controlled by the type of adhesive molecules involved, and their affinity to the extra–cellular–matrix, this work is presently under way.

5 Conclusions

The motility of two types of epithelial bladder cancer cells has been investigated from a biophysical point of view. These cells present different invasive behavior, in particular T24 cells are more invasive than the other kind (RT112). Substrates of PolyAcrylamide (10 kPa) have been chosen to perform all studies. The main results of this study concern the relationship between focal areas, cytoskeleton structure, migration velocities and forces exerted by cells thanks to Traction Force Microscopy (TFM). The main conclusions are that invasive cells (T24) need less traction forces to

migrate, and exhibit an organized cytoskeleton (actin and myosin structures) with large adhesion sites, resulting in larger migration velocities on this particular substrate. On the other hand, less invasive RT112 cells exert larger forces thanks to a wide acto–myosin cortex, with smaller focal adhesions. The applications of this method could be an interesting *in vitro* tool to test the invasivity of different cancer cells; in particular, the role of traction stress may provide a possible discrimination criterion.

Future studies could focus on the optimization of protocols (choice of substrate, functionnalization, topography) for achieving such studies, and the use of high numbers of cells for designing more efficient protocols. Finally, promising current work is ongoing to relate the possible proteins involved in cancer migration of such cells [10, 25], like $\beta 1$ integrins [28] or $\alpha 5 - \beta 1$ [38] and more precisely chemokine CXCL1 in the case of the two lines studied here [30]. This would enhance the current results on the traction forces measured here by TFM. Possibly this could also enable models [40, 57, 27, 51, 16] to predict cancer cell shapes during migration.

6 Acknowledgments

V. Peschetola is thankful to the Université Franco–Italienne for sponsorship. This work was partly funded by the European Commission (EC) through a Marie Curie Research Training Network (MRTN–CT–2004–503661) entitled Modeling, mathematical methods and computer simulation of tumor growth and therapy. Confocal microscopy was performed at the microscopy facility of the Institut Albert Bonniot. This latter equipment was partly funded by the "Association pour la Recherche sur le Cancer" (ARC, Villejuif, France) and the Nanobio program (Nanosciences Foundation, Grenoble). We thank Olivier Destaing, for help with the transfection of actin–GFP.

References

[1] D. Ambrosi. Cellular cellular traction as an inverse problem. *SIAM J. Appl. Math.*, 66:2049–2060, 2006.

[2] D. Ambrosi, A. Duperray, V. Peschetola, and C. Verdier. Traction patterns of tumor cells. *J. Math. Biol.*, 58:163–181, 2009.

[3] Y. Aratyn-Schaus and M. L. Gardel. Transient frictional slip between integrin and the ecm in focal adhesions under myosin ii tension. *Curr. Biol.*, 20(13):1145–1153, 2010.

[4] N. Q. Balaban, U. S. Schwarz, D. Riveline, P. Goichberg, G. Tzur, I. Sabanay, D. Mahalu, S. Safran, A. Bershadsky, L. Addadi, and B. Geiger. Force and focal adhesion assembly: a close relationship studied using elastic micropatterned substrates. *Nat. Cell Biol.*, 3(5):466–472, 2001.

[5] E. M. Bindels, M. Vermey, N. J. De Both, and T. H. van der Kwast. Influence of the microenvironment on invasiveness of human bladder carcinoma cell lines. *Virchows Arch.*, 439(4):552–559, 2001.

[6] K. Burton, J. H. Park, and D. L. Taylor. Keratocytes generate traction forces in two phases. *Mol. Biol. Cell*, 10(11):3745–3769, Nov 1999.

[7] K. Burton and D. L. Taylor. Traction forces of cytokinesis measured with optically modified elastic substrata. *Nature*, 385(6615):450–454, 1997.

[8] J. P. Butler, I. M. Tolic-Norrelykke, B. Fabry, and J. J. Fredberg. Traction fields, moments, and strain energy that cells exert on their surroundings. *Am. J. Physiol. Cell Physiol.*, 282(3):C595–C605, 2002.

[9] D. Choquet, D. P. Felsenfeld, and M. P. Sheetz. Extracellular matrix rigidity causes strengthening of integrin-cytoskeleton linkages. *Cell*, 88(1):39–48, 1997.

[10] R. Chotard-Ghodsnia, O. Haddad, A. Leyrat, A. Drochon, C. Verdier, and A. Duperray. Morphological analysis of tumor cell/endothelial cell interactions under shear flow. *J. Biomech.*, 40(2):335–344, 2007.

[11] C. Couzon, A. Duperray, and C. Verdier. A critical stress to detach cancer cells in microchannels. *Eur. Biophys. J.*, 38:1035–1047, 2009.

[12] H. Delanoë-Ayari, J.-P. Rieu, and M. Sano. 4d traction force microscopy reveals asymmetric cortical forces in migrating dictyostelium cells. *Phys. Rev. Lett.*, 105:248103, 2010.

[13] M. Dembo and Y. L. Wang. Stresses at the cell-to-substrate interface during locomotion of fibroblasts. *Biophys. J.*, 76(4):2307–2316, 1999.

[14] P. Dieterich, R. Klages, R. Preuss, and A. Schwab. Anomalous dynamics of cell migration. *Proc. Natl. Acad. Sci. USA*, 105(2):459–463, 2008.

[15] D. E. Discher, P. Janmey, and Y.-L. Wang. Tissue cells feel and respond to the stiffness of their substrate. *Science*, 310(5751):1139–1143, 2005.

[16] J. Etienne and A. Duperray. Initial dynamics of cell spreading are governed by dissipation in the actin cortex. *Biophys. J.*, 101(3):611–621, 2011.

[17] M. F. Fournier, R. Sauser, D. Ambrosi, J.-J. Meister, and A. B. Verkhovsky. Force transmission in migrating cells. *J. Cell Biol.*, 188(2):287–297, 2010.

[18] P. Friedl, S. Borgmann, and E. B. Brcker. Amoeboid leukocyte crawling through extracellular matrix: lessons from the dictyostelium paradigm of cell movement. *J. Leukoc. Biol.*, 70(4):491–509, 2001.

[19] C. G. Galbraith, K. M. Yamada, and M. P. Sheetz. The relationship between force and focal complex development. *J. Cell Biol.*, 159(4):695–705, 2002.

[20] M. L. Gardel, B. Sabass, L. Ji, G. Danuser, U. S. Schwarz, and C. M. Waterman. Traction stress in focal adhesions correlates biphasically with actin retrograde flow speed. *J. Cell Biol.*, 183(6):999–1005, 2008.

[21] M. Ghibaudo, A. Saez, L. Trichet, A. Xayaphoummine, J. Browaeys, P. Silberzan, A. Buguin, and B. Ladoux. Traction forces and rigidity sensing regulate cell functions. *Soft Matter*, 4:1836–1843, 2008.

[22] M. Ghibaudo, L. Trichet, J. L. Digabel, A. Richert, P. Hersen, and B. Ladoux. Substrate topography induces a crossover from 2d to 3d behavior in fibroblast migration. *Biophys. J.*, 97(1):357–368, 2009.

[23] G. Giannone, B. J. Dubin-Thaler, O. Rossier, Y. Cai, O. Chaga, G. Jiang, W. Beaver, H.-G. Dbereiner, Y. Freund, G. Borisy, and M. P. Sheetz. Lamellipodial actin mechanically links myosin activity with adhesion-site formation. *Cell*, 128(3):561–575, 2007.

[24] S. L. Gupton and C. M. Waterman-Storer. Spatiotemporal feedback between actomyosin and focal–adhesion systems optimizes rapid cell migration. *Cell*, 125(7):1361–1374, 2006.

[25] O. Haddad, R. Chotard-Ghodsnia, C. Verdier, and A. Duperray. Tumor cell/endothelial cell tight contact upregulates endothelial adhesion molecule expression mediated by nfkb: differential role of the shear stress. *Exp. Cell Research*, 316:615–626, 2010.

[26] A. K. Harris, P. Wild, and D. Stopak. Silicone rubber substrata: a new wrinkle in the study of cell locomotion. *Science*, 208:177–179, 1980.

[27] M. Herant and M. Dembo. Form and function in cell motility: from fibroblasts to keratocytes. *Biophys. J.*, 98(8):1408–1417, 2010.

[28] I. Indra, V. Undyala, C. Kandow, U. Thirumurthi, M. Dembo, and K. A. Beningo. An in vitro correlation of mechanical forces and metastatic capacity. *Phys. Biol.*, 8(1):015015, 2011.

[29] A. Iordan, A. Duperray, A. Grard, A. Grichine, and C. Verdier. Breakdown of cell-collagen networks through collagen remodeling. *Biorheology*, 47:277–295, 2010.

[30] H. Kawanishi, Y. Matsui, M. Ito, J. Watanabe, T. Takahashi, K. Nishizawa, H. Nishiyama, T. Kamoto, Y. Mikami, Y. Tanaka, G. Jung, H. Akiyama, H. Nobumasa, P. Guilford, A. Reeve, Y. Okuno, G. Tsujimoto, E. Nakamura, and O. Ogawa. Secreted cxcl1 is a potential mediator and marker of the tumor invasion of bladder cancer. *Clin. Cancer Res.*, 14(9):2579–2587, 2008.

[31] K. Keren, Z. Pincus, G. M. Allen, E. L. Barnhart, G. Marriott, A. Mogilner, and J. A. Theriot. Mechanism of shape determination in motile cells. *Nature*, 453(7194):475–480, 2008.

[32] C. M. Kraning-Rush, J. P. Califano, and C. A. Reinhart-King. Cellular traction stresses increase with increasing metastatic potential. *Plos One*, 7(2):e32572, 2012.

[33] L. Landau and E. Lisfchitz. *Théorie de l'élasticité.* Editions Mir, 1967.

[34] W. R. Legant, J. S. Miller, B. L. Blakely, D. M. Cohen, G. M. Genin, and C. S. Chen. Measurement of mechanical tractions exerted by cells in three-dimensional matrices. *Nat. Methods*, 7(12):969–971, 2010.

[35] J. L. Lions. *Contrôle optimal de systèmes gouvernés par des équations aux dérivées partielles.* Dunod, Paris, 1968.

[36] C. M. Lo, H. B. Wang, M. Dembo, and Y. L. Wang. Cell movement is guided by the rigidity of the substrate. *Biophys. J.*, 79(1):144–152, 2000.

[37] S. A. Maskarinec, C. Franck, D. A. Tirrell, and G. Ravichandran. Quantifying cellular traction forces in three dimensions. *Proc. Natl. Acad. Sci. USA*, 106(52):22108–22113, 2009.

[38] C. T. Mierke, B. Frey, M. Fellner, M. Herrmann, and B. Fabry. Integrin alpha5–beta1 facilitates cancer cell invasion through enhanced contractile forces. *J. Cell Sci.*, 124(3):369–383, 2011.

[39] C. T. Mierke, D. Rösel, B. Fabry, and J. Brábek. Contractile forces in tumor cell migration. *Eur. J. Cell Biol.*, 87:669–676, 2008.

[40] A. Mogilner and K. Keren. The shape of motile cells. *Current Biology*, 19:R762–R771, 2009.

[41] S. Munevar, Y. Wang, and M. Dembo. Traction force microscopy of migrating normal and h-ras transformed 3t3 fibroblasts. *Biophys. J.*, 80(4):1744–1757, 2001.

[42] S. P. Palecek, J. C. Loftus, M. H. Ginsberg, D. A. Lauffenburger, and A. F. Horwitz. Integrin-ligand binding properties govern cell migration speed through cell-substratum adhesiveness. *Nature*, 385(6616):537–540, 1997.

[43] R. Paul, P. Heil, J. P. Spatz, and U. S. Schwarz. Propagation of mechanical stress through the actin cytoskeleton toward focal adhesions: model and experiment. *Biophys. J.*, 94(4):1470–1482, 2008.

[44] R. J. Pelham and Y. Wang. High resolution detection of mechanical forces exerted by locomoting fibroblasts on the substrate. *Mol. Biol. Cell*, 10(4):935–945, 1999.

[45] V. Peschetola. *Traction forces exerted by cancer cells migrating on gels*. PhD thesis, Université de Grenoble, 2011.

[46] T. D. Pollard and G. G. Borisy. Cellular motility driven by assembly and disassembly of actin filaments. *Cell*, 112(4):453–465, 2003.

[47] W. S. Rasband. *ImageJ*. U.S. National Institutes of Health, Bethesda, Maryland, USA, 1997–2007.

[48] B. Sabass, M. L. Gardel, C. M. Waterman, and U. S. Schwarz. High resolution traction force microscopy based on experimental and computational advances. *Biophys. J.*, 94(1):207–220, 2008.

[49] A. Saez, M. Ghibaudo, A. Buguin, P. Silberzan, and B. Ladoux. Rigidity-driven growth and migration of epithelial cells on microstructured anisotropic substrates. *Proc. Natl. Acad. Sci. USA*, 104(20):8281–8286, 2007.

[50] U. S. Schwarz, N. Q. Balaban, D. Riveline, A. Bershadsky, B. Geiger, and S. A. Safran. Calculation of forces at focal adhesions from elastic substrate data: the effect of localized force and the need for regularization. *Biophys. J.*, 83(3):1380–1394, 2002.

[51] D. Shao, W.-J. Rappel, and H. Levine. Computational model for cell morphodynamics. *Phys. Rev. Lett.*, 105:108104, 2010.

[52] M. P. Sheetz, D. P. Felsenfeld, and C. G. Galbraith. Cell migration: regulation of force on extracellular-matrix-integrin complexes. *Trends Cell Biol.*, 8(2):51–54, 1998.

[53] J. Stricker, Y. Aratyn-Schaus, P. W. Oakes, and M. L. Gardel. Spatiotemporal constraints on the force-dependent growth of focal adhesions. *Biophys. J.*, 100(12):2883–2893, 2011.

[54] J. Stricker, B. Sabass, U. S. Schwarz, and M. L. Gardel. Optimization of traction force microscopy for micron-sized focal adhesions. *J. Phys. Condens. Matter*, 22(19):194104, 2010.

[55] J. L. Tan, J. Tien, D. M. Pirone, D. S. Gray, K. Bhadriraju, and C. S. Chen. Cells lying on a bed of microneedles: an approach to isolate mechanical force. *Proc. Natl. Acad. Sci. USA*, 100(4):1484–1489, 2003.

[56] Q. Tseng, I. Wang, E. Duchemin-Pelletier, A. Azioune, N. Carpi, J. Gao, O. Filhol, M. Piel, M. Théry, and M. Balland. A new micropatterning method of soft substrates reveals that different tumorigenic signals can promote or reduce cell contraction levels. *Lab. Chip*, 11(13):2231–2240, 2011.

[57] C. Verdier, J. Etienne, A. Duperray, and L. Preziosi. Review: Rheological properties of biological materials. *C. R. Acad. Sci. Phys.*, 10:790–811, 2009.

[58] M. Versaevel, T. Grevesse, and S. Gabriele. Spatial coordination between cell and nuclear shape within micropatterned endothelial cells. *Nature Comm.*, 3(671):1–12, 2012.

Figure captions and Movies

Figure 1. Phase–contrast image of a T24 cancer cell (at time $t = 6$ min from Fig. 2) and corresponding traction field of a T24 cell represented as a color map. The color scale for stresses reads in Pascal (Pa).

Figure 2. Time variation of the magnitude of traction stresses exerted by a T24 migrating cancer cell as a Boxplot. The lines in the Boxplot correspond to 25%, 50%, 75%, and the whiskers extend to the 1.5 interquartile range. Outliers are above. The mean value for each time step is indicated by the red dots.

Figure 3. Phase–contrast image of a RT112 cancer cell (at time $t = 18$ min from Fig. 4) and corresponding traction field of a RT112 cell represented as a color map. The color scale for stresses reads in Pascal (Pa).

Figure 4. Time variation of the magnitude of traction stresses exerted by a RT112 migrating cancer cell as a Boxplot. The lines in the Boxplot correspond to 25%, 50%, 75%, and the whiskers extend to the 1.5 interquartile range. Outliers are above. The mean value for each time step is indicated by the red dots.

Figure 5. Mean value of the outliers of traction stresses for T24 and RT112 cell lines. The data is shown as the mean + standard error about the mean (SEM). The difference among the mean value is significant according to the GEE test ($p = 0.0069$).

Figure 6. Stresses in a half–T24 cell and the resultant (arrow). Stresses in a half–RT112 cell. Bar–plot showing time-average force in the direction of migration ($p = 0.14$).

Figure 7. Fluorescent images of T24 cancer cells adhering on PA gel (10kPa). From left to right and top to bottom: cells are stained for actin with Phalloidin Alexa 488 (green), anti–paxillin for focal adhesion sites (red), anti–myosin antibody for myosin IIA (magenta) and Hoechst for nuclei (blue).

Figure 8. Fluorescent images of RT112 cancer cells adhering on PA gel (10kPa). From left to right and top to bottom: cells are stained for actin with Phalloidin Alexa 488 (green), anti–paxillin for focal adhesion sites (red), anti–myosin antibody for myosin IIA (magenta) and Hoechst for nuclei (blue).

Figure 9. (A) Image of focal adhesions. (B) Details of segmentation procedure for focal adhesions calculation – Bar–plot representing total area of focal complexes (>0.5 µm^2) divided by cell area ($p = 0.25$). See also Table 1 for details.

Figure 10. Image of T24 cancer cell transfected for actin on a PA gel substrate (10kPa). Fluorescent image with line (at the front) indicating the level of actin expression and corresponding

traction force map (in Pa).

Figure 11. Image of RT112 cancer cell transfected for actin on a PA gel substrate (10kPa). Fluorescent image with line (at the front) indicating the level of actin expression and corresponding traction force map (in Pa).

Figure 12. Co–localization of the actin and force levels. T24 cell (top) and RT112 cell (below). Larger actin areas are found with the RT112 cell.

Supplemental movie S1. Phase–contrast movie of a migrating T24 cancer cell (one image every 2 minutes).

Supplemental movie S2. Corresponding traction field of the migrating T24 cell represented as a color map. The color scale for stresses reads in Pascal (one image every 2 minutes).

Supplemental movie S3. Phase–contrast movie of a migrating RT112 cancer cell (one image every 4 minutes).

Supplemental movie S4. Corresponding traction field of the migrating RT112 cell represented as a color map. The color scale for stresses reads in Pascal (one image every 4 minutes).

Supplemental movie S5. Colocalization map of actin fibers and stress magnitude for migrating T24 cell (one image every 2 minutes).

Supplemental movie S6. Colocalization map of actin fibers and stress magnitude for migrating RT112 cell (one image every 2 minutes).

Figures

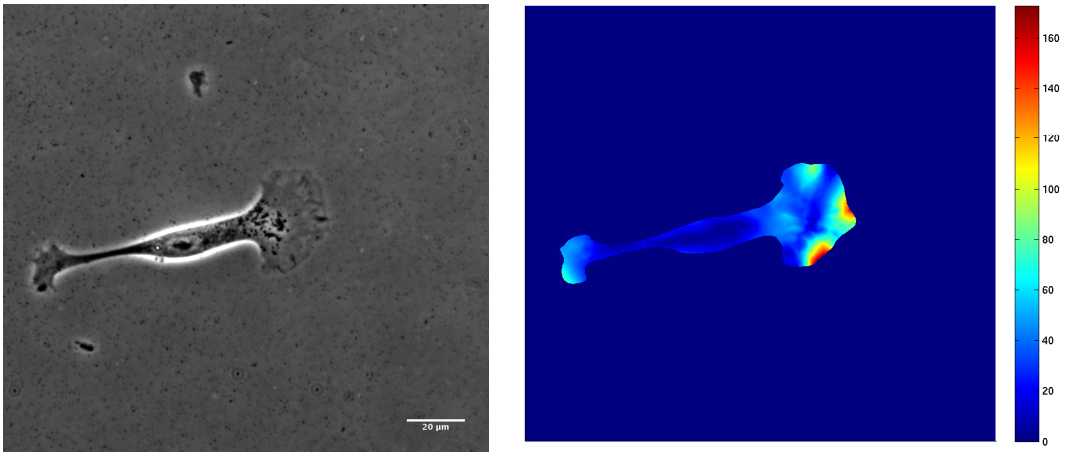

Figure 1: Phase–contrast image of a T24 cancer cell (at time $t = 6$ min from Fig. 2) and corresponding traction field of a T24 cell represented as a color map. The color scale for stresses reads in Pascal (Pa).

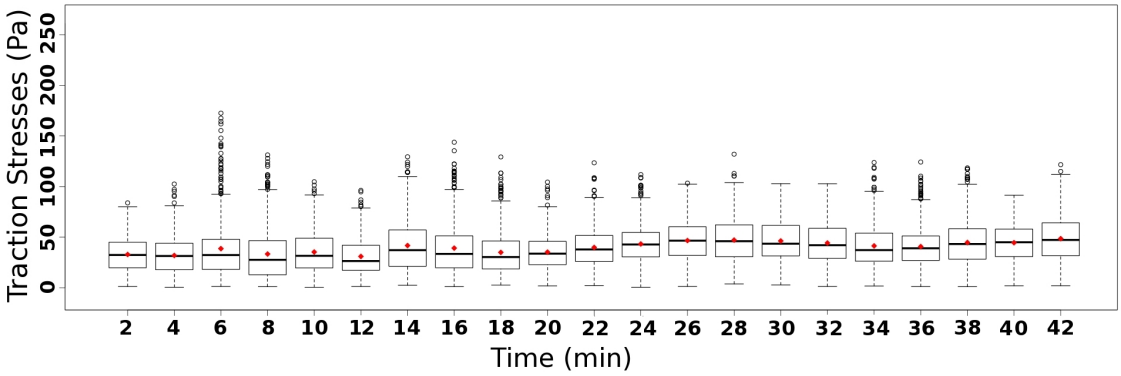

Figure 2: Time variation of the magnitude of traction stresses exerted by a T24 migrating cancer cell as a Boxplot. The lines in the Boxplot correspond to 25%, 50%, 75%, and the whiskers extend to the 1.5 interquartile range. Outliers are above. The mean value for each time step is indicated by the red dots.

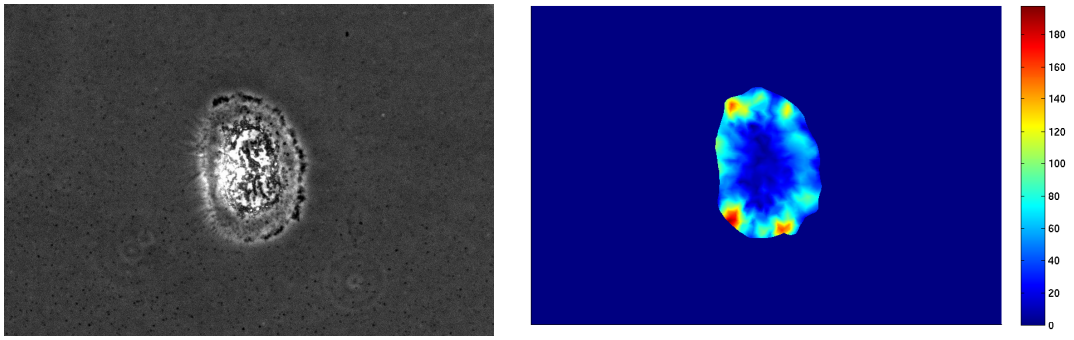

Figure 3: Phase–contrast image of a RT112 cancer cell (at time $t = 18$ min from Fig. 4) and corresponding traction field of a RT112 cell represented as a color map. The color scale for stresses reads in Pascal (Pa).

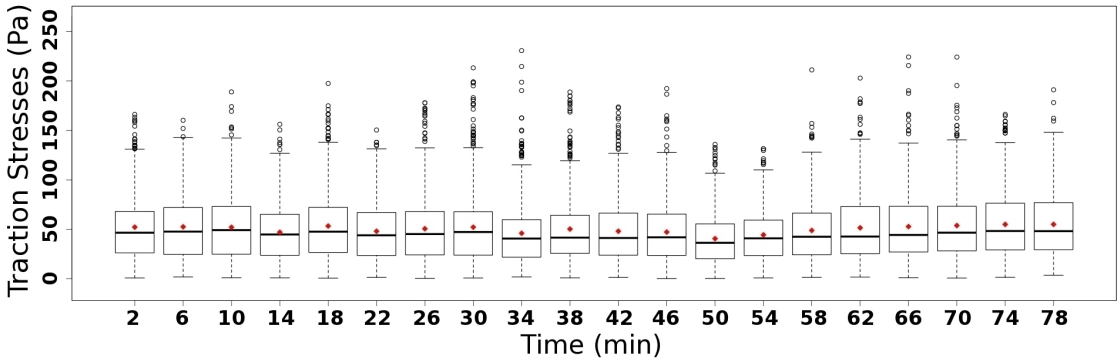

Figure 4: Time variation of the magnitude of traction stresses exerted by a RT112 migrating cancer cell as a Boxplot. The lines in the Boxplot correspond to 25%, 50%, 75%, and the whiskers extend to the 1.5 interquartile range. Outliers are above. The mean value for each time step is indicated by the red dots.

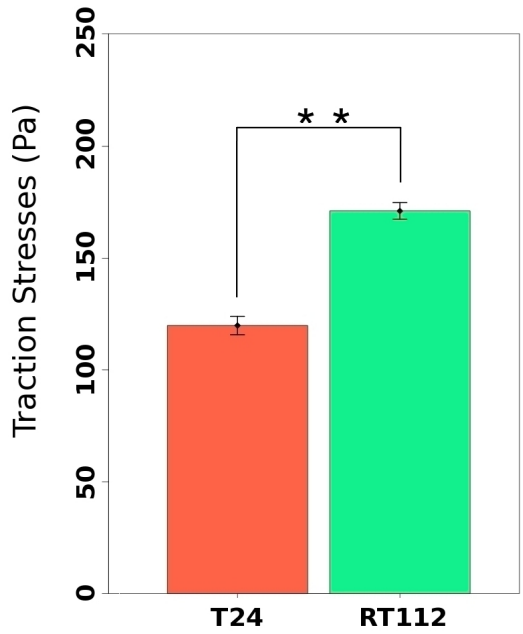

Figure 5: Mean value of the outliers of traction stresses for T24 and RT112 cell lines. The data is shown as the mean + standard error about the mean (SEM). The difference among the mean value is significant according to the GEE test ($p = 0.0069$).

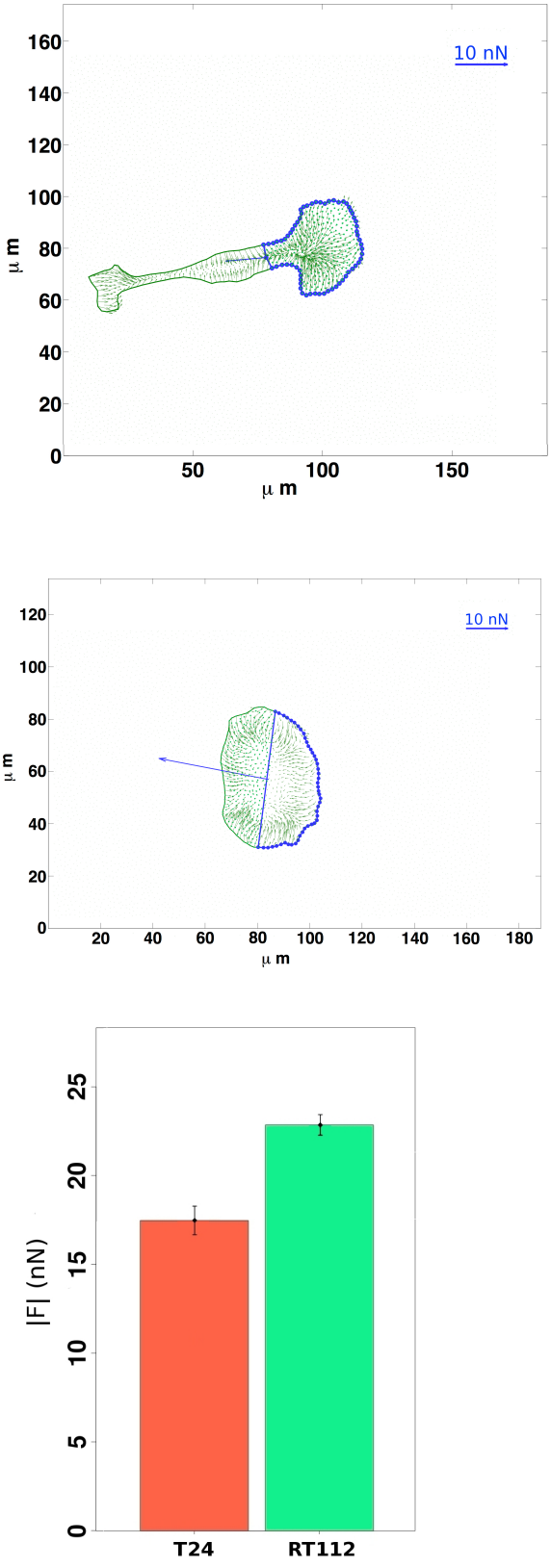

Figure 6: Stresses in a half–T24 cell and the resultant (arrow). Stresses in a half–RT112 cell. Bar–plot showing time-average force in the direction of migration ($p = 0.14$).

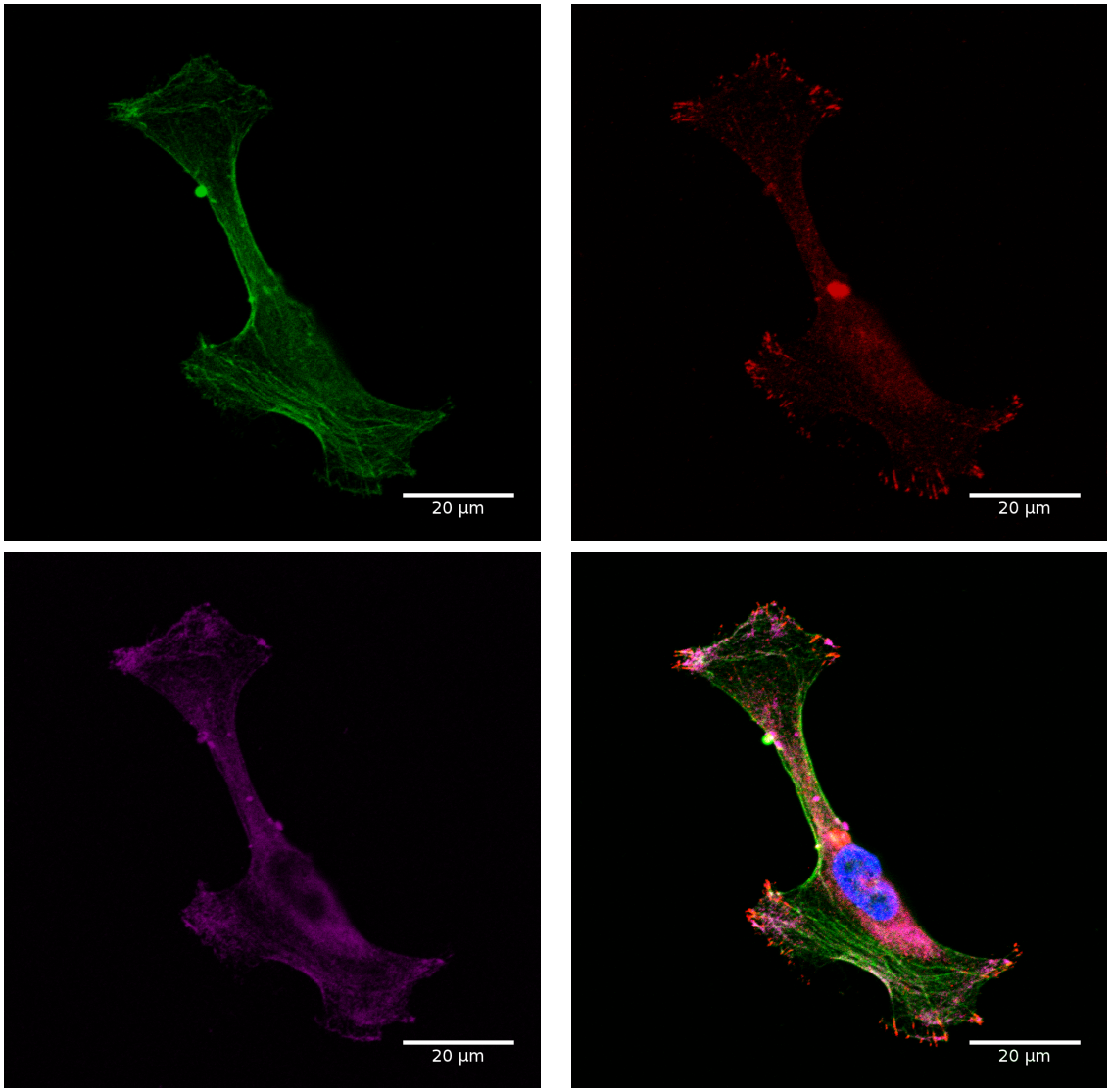

Figure 7: Fluorescent images of T24 cancer cells adhering on PA gel (10kPa). From left to right and top to bottom: cells are stained for actin with Phalloidin Alexa 488 (green), anti–paxillin for focal adhesion sites (red), anti–myosin antibody for myosin IIA (magenta) and Hoechst for nuclei (blue).

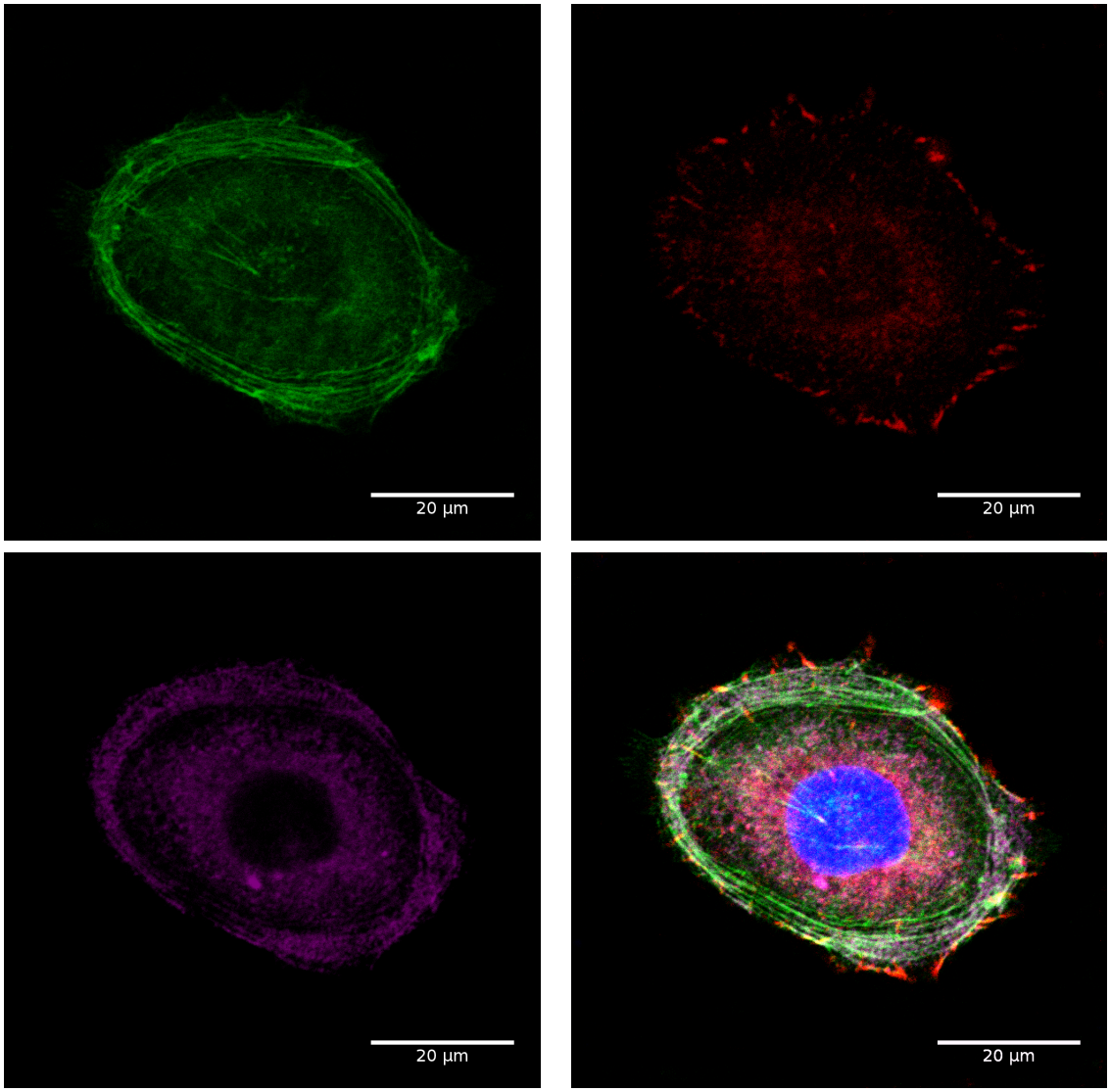

Figure 8: Fluorescent images of RT112 cancer cells adhering on PA gel (10kPa). From left to right and top to bottom: cells are stained for actin with Phalloidin Alexa 488 (green), anti–paxillin for focal adhesion sites (red), anti–myosin antibody for myosin IIA (magenta) and Hoechst for nuclei (blue).

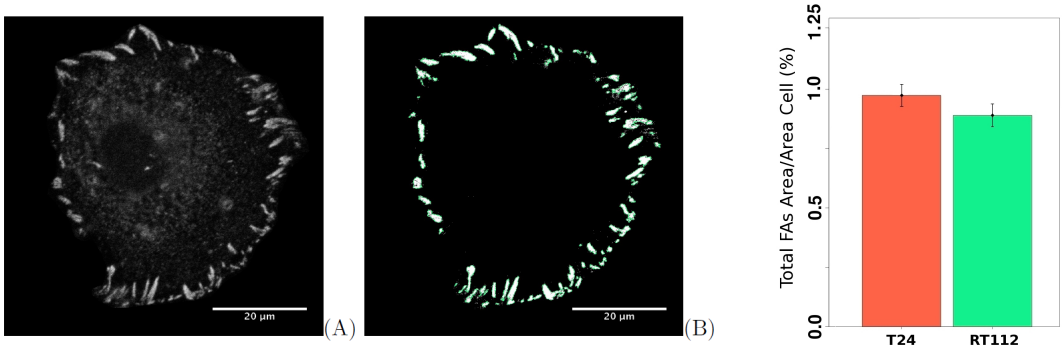

(A) (B)

Figure 9: (A) Image of focal adhesions. (B) Details of segmentation procedure for focal adhesions calculation – Bar–plot representing total area of focal complexes (>0.5 µm^2) normalized by cell area ($p = 0.25$). See also Table 1 for details.

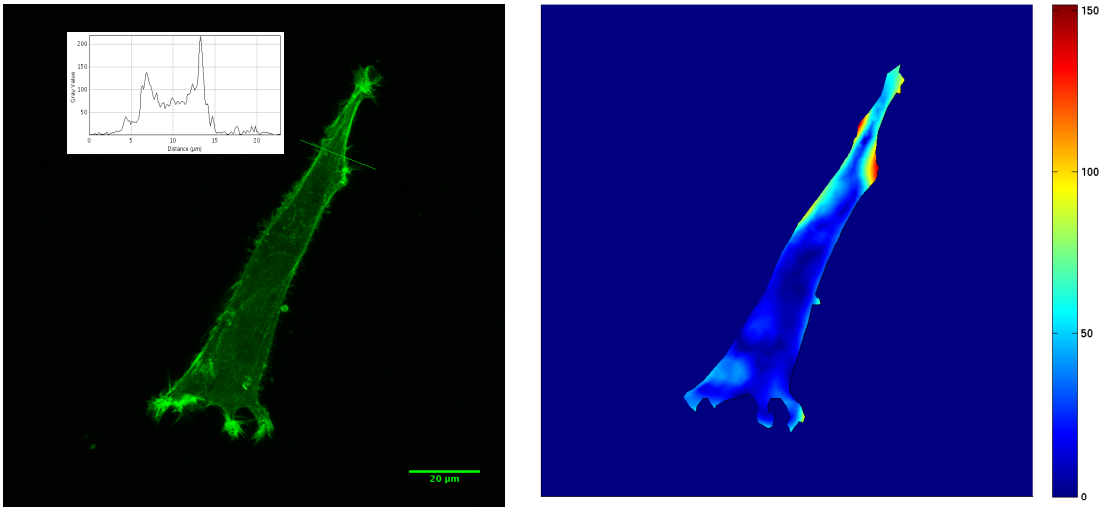

Figure 10: Image of T24 cancer cell transfected for actin on a PA gel substrate (10kPa). Fluorescent image with line (at the front) indicating the level of actin expression and corresponding traction force map (in Pa).

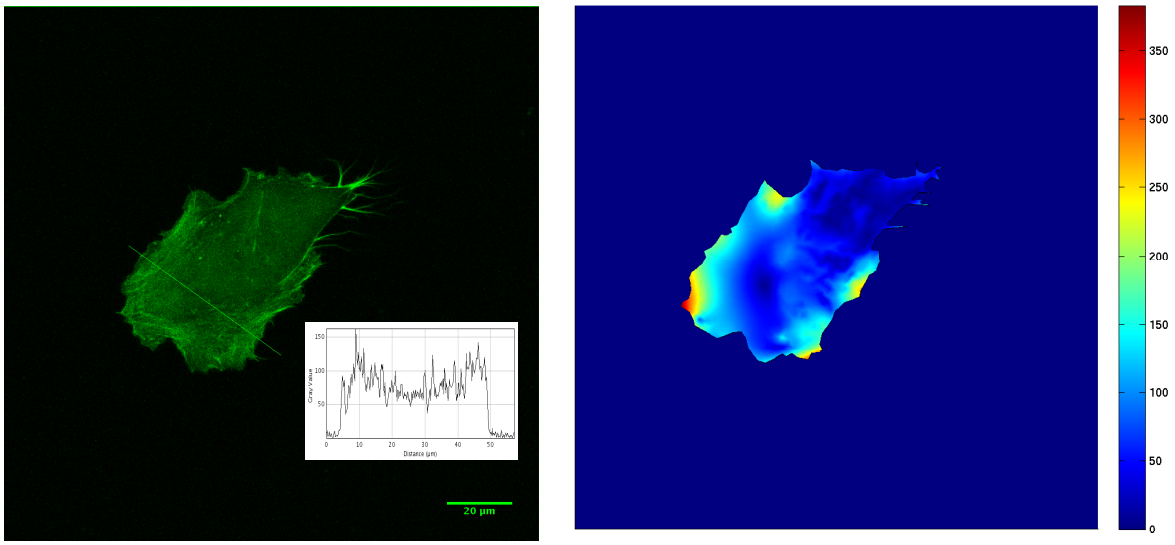

Figure 11: Image of RT112 cancer cell transfected for actin on a PA gel substrate (10kPa). Fluorescent image with line (at the front) indicating the level of actin expression and corresponding traction force map (in Pa).

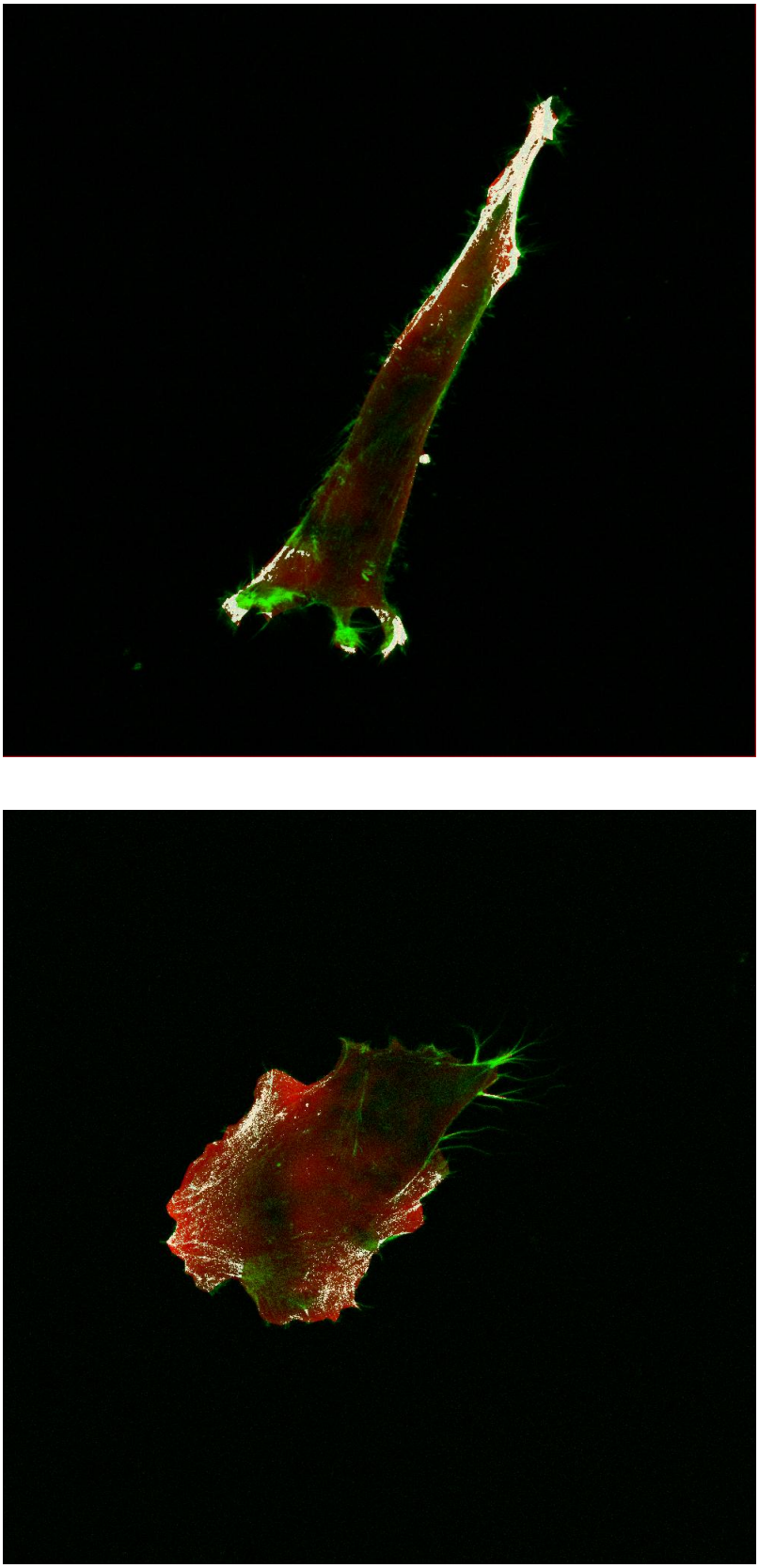

Figure 12: Co–localization of the actin and force levels. T24 cell (top) and RT112 cell (below). Larger actin areas are found with the RT112 cell.